

Surface vibrations in alkanethiol self-assembled monolayers of varying chain length

A. W. Rosenbaum, M. A. Freedman, S. B. Darling,^{a)} I. Popova, and S. J. Sibener^{b)}

The James Franck Institute and Department of Chemistry, The University of Chicago, Chicago, Illinois 60637

(Received 19 September 2003; accepted 24 November 2003)

The effect of chain length on the low-energy vibrations of alkanethiol striped phase self-assembled monolayers on Au(111) was studied. We have examined the low-energy vibrational structure of well-ordered, low-density 1-decanethiol (C10), 1-octanethiol (C8), and 1-hexanethiol (C6) to further understand the interaction between adsorbate and substrate. Dispersionless Einstein mode phonons, polarized perpendicularly to the surface, were observed for the striped phases of C10, C8, and C6 at 8.0, 7.3, and 7.3 meV, respectively. An overtone at 12.3 meV was also observed for C6/Au(111). These results, in concert with molecular dynamics simulations, indicate that the forces between the adsorbate and substrate can be described using simple van der Waals forces between the hydrocarbon chains and the Au substrate with the sulfur chemisorbed in the threefold hollow site.

© 2004 American Institute of Physics. [DOI: 10.1063/1.1643353]

I. INTRODUCTION

Self-assembled monolayers (SAMs) formed from organic thiols on Au(111) have been studied extensively for over a decade.^{1–5} The strong interest in SAMs comes from their robust potential for many chemical, physical, and biological applications. The surface chemistry and structure of a SAM can be tuned by changing functional groups. Tying these powerful properties of self-organization and adaptability together, SAMs have been used for lithography, tribology, nano-electronic and biological sensor applications.^{6–8} Alkanethiol SAMs in particular have been studied as a model system for self-assembly. Fundamental studies have focused on the structural phase diagram of alkanethiol SAMs. Two basic phases have been found to be prevalent, a high-density $c(4\times 2)$ phase formed from large exposures to the alkanethiol, in solution or via vapor deposition, and a low-density ($p\times\sqrt{3}$) phase created with smaller doses. There are a variety of other intermediate and low-density phases, which have varying degrees of overlap between alkanethiol chains.^{3,9} The low-density striped phases studied here are all the lowest density phase for that particular chain length.

To better understand the self-assembly process it is necessary to delve deeper into the molecular interactions. Helium atom scattering is a unique tool that can be used to gain insight into the dynamics of monolayers and thin films without damaging the adsorbates. This technique has been used in the past to study thin organic films. For example, Fuhrmann *et al.* have shown it is possible to extract information about friction forces from vibrations of alkane monolayers on Cu(111).¹⁰ Other comparable studies have been used to advance theories on phase transitions, adsorbate diffusion, and energy exchange.^{11–14}

The majority of these scattering studies have been conducted on physisorbed species, such as alkanes or alkanethiols on Au(111) or Cu(111).^{15–18} Of particular interest due to their similarity to SAMs are alkanes/Cu(111) and physisorbed alkanethiols/Cu(100) which have been found to have low-energy FT_z vibrational modes at 7.2 and 6.0 meV, respectively, that are independent of chain length.^{19,20} This FT_z vibrational mode has also been found to exist in a chemisorbed 1-decanethiol SAM.⁵ In this paper we look at the effects of varying the chain length of chemisorbed alkanethiols on Au(111). By doing this we aim to expand our comprehension of the influence of the chemisorbed sulfur group. This experiment will also help to better characterize the chain–chain and chain–substrate interactions that control the self-assembly process.

II. EXPERIMENT

Experiments were conducted in a high momentum- and energy-resolution helium atom scattering apparatus. Elastic and inelastic scattering events are observed through diffraction and time-of-flight (TOF) measurements, respectively. This instrument has been described in detail elsewhere, and its design will only be summarized here.^{21,22} It consists of a cryogenically cooled supersonic helium beam source, an UHV scattering chamber equipped with appropriate surface characterization tools (such as LEED, Auger, etc.), a pre-collision chopper (chopper to sample distance of 1.554 m), and a rotating, long flight path (sample to ionizer distance of 1.005 m) quadrupole mass spectrometer detector. The angular collimation yields a resolution of 0.22° and the $\Delta v/v$ for most beam energies used is less than 1%. The Au(111) crystal used in these studies was cleaned by repeated cycles of sputtering with 0.5 keV Ne^+ ions followed by annealing above 750 K until contaminant levels were below our Auger detection limit and helium reflectivity was maximized. Sur-

^{a)}Present address: Materials Science Division, Argonne National Laboratory, 9700 South Cass Avenue, Argonne, Illinois 60439.

^{b)}Author to whom correspondence should be addressed. Electronic mail: s-sibener@uchicago.edu

TABLE I. A listing of parameters for the VENUS intermolecular potential. The stretch parameters (k_r and r_0) are in mdyne/Å and Å. The bend parameters (k_θ and θ) are in mdyne Å/rad² and deg. The dihedral parameters (k and ϕ) are in kcal/mol and deg. The Lennard-Jones parameters (a , b , ϵ , and σ) are in kcal/mol Å¹², kcal/mol Å⁶, kcal/mol, and Å.

Interaction	Parameter
C-C stretch	$k_r=4.86$, $r_0=1.53$
C-S Stretch	$k_r=5.70$, $r_0=1.82$
C-C-C Bend	$k_\theta=0.862$, $\theta_0=109.5$
C-C-S Bend	$k_\theta=0.862$, $\theta_0=114.0$
Dihedral C-C-C-C or S-C-C-C	$k_1=3.705$, $\phi_1=0$, $k_2=-0.135$, $\phi_2=180$, $k_3=1.571$, $\phi_3=0$
CH ₂ -CH ₃ Lennard-Jones	$a=7204000$, $b=2032$
CH ₂ -CH ₂ Lennard-Jones	$a=5915000$, $b=1668$
CH ₂ -S Lennard-Jones	$a=4859000$, $b=1825$
CH ₃ -S Lennard-Jones	$a=5917000$, $b=2226$
CH ₂ & CH ₃ -Au Lennard-Jones	$\sigma=3.28$, $\epsilon=0.429$

face crystallinity was confirmed by helium diffraction from the ($23\times\sqrt{3}$) Au reconstruction with average domain sizes greater than 400 Å.

Alkanethiols (1-decanethiol, 1-octanethiol, and 1-hexanethiol) were purified by repeated freeze-pump-thaw cycles and dosed by backfilling the scattering chamber, from a base pressure of 10^{-10} Torr to pressures of approximately 10^{-8} Torr. High quality striped phase SAMs with domain sizes as large as the underlying gold terraces were prepared by dosing at a surface temperature of 280 K followed by a 10 min anneal below the desorption temperature (~ 400 K). Diffraction scans from the SAMs were obtained at surface temperatures of 80 K to optimize the signal to noise ratio of the elastic diffraction by minimizing Debye-Waller attenuation. TOF spectra for C10, C8, and C6 were taken at a surface temperature of 100 K to increase the excited vibrational population thereby increasing the probability of an annihilation event. The surface temperature of C6 was varied for Debye-Waller measurements and TOF spectra to probe the dependence of the overtone's intensity on temperature. All data were recorded with scattering along the $\langle 110 \rangle$ azimuth.

Normal modes analysis of the SAMs was performed using the molecular dynamics code VENUS.^{23,24} The potential energy surface was created using a united atom method and a simple force field potential to account for the harmonic stretches, dihedral angles, and Lennard-Jones interaction,

$$\begin{aligned}
 V = & \sum_{\text{stretches}} k_r \frac{(r-r_0)^2}{2} + \sum_{\text{bends}} k_\theta \frac{(\theta-\theta_0)^2}{2} \\
 & + \sum_{\text{dihedrals}} \sum_{n=1}^3 k_n \frac{[1 + \cos(n\phi - \phi_n)]}{2} \\
 & + \sum_{\text{Lennard-Jones}} (a/r^{12} - b/r^6). \quad (1)
 \end{aligned}$$

The parameters used, shown in Table I, were taken from prior theoretical work on SAMs and alkane films on gold.^{14,25}

The system is modeled with a single thiol chain with the sulfur chemically bound in the threefold hollow site of a

Au(111) surface with the chain parallel to the surface and running along the $\langle 110 \rangle$ direction. This adsorption site and chain orientation agree with experimental and theoretical studies of low-density alkanethiols on Au(111).^{26,27} While holding the Au surface atoms rigid, the thiol chain position is energetically minimized. An analysis at a surface temperature of 0 K with no zero point energy was used to extract the vibrational frequencies and modes for the different chain lengths. Since the vibrational modes of interest are low in energy, state populations were assumed to be sufficiently large at temperatures of 100 K to allow for experimental annihilation events and verified via Boltzmann distribution calculations. While experimental data were collected only for C6, C8, and C10, normal modes calculations were performed for 1-butanethiol (C4) and 1-dodecanethiol (C12) along with C6, C8, and C10.

III. RESULTS

The structural characterization of the C10 ($11.5\times\sqrt{3}$) low-density phase on Au(111) is shown in Fig. 1(a). The striped phase was created via vapor deposition of ~ 20 L of C10 onto the reconstructed Au(111) and exhibited domain sizes larger than 400 Å after annealing near the desorption temperature (~ 400 K). After confirming the quality of the C10 SAM by helium atom diffraction, the sample temperature was raised to 100 K for inelastic scattering. A representative TOF spectrum [Fig. 1(b)] and a dispersion plot [Fig. 1(c)] constructed from the data are also shown. The structure and vibrational modes of C10 have been explored previously.^{5,28} The vibration was identified as an Einstein mode with an energy of 8.0 ± 0.3 meV and assigned as a frustrated translation perpendicular to the surface, FT_z .

Further studies were conducted on the C8 striped phase, ($10\times\sqrt{3}$), on Au(111). The striped phase of C8 also exhibited domains larger than 400 Å. Figure 2 shows a representative diffraction scan from the C8/Au(111) striped phase as well as inelastic data in which a single dispersionless phonon event was observed. The beam energy was varied to optimize the signal to noise ratio of the single phonon scattering. The energy of the creation and annihilation events was $\Delta E = 7.3 \pm 0.2$ meV and this mode is identified as a FT_z phonon in agreement with prior work on alkanethiols and alkanes on a variety of substrates.^{5,19,20}

Data for the C6/Au(111) SAM system are shown in Fig. 3. The diffraction in the $\langle 110 \rangle$ direction matches the 0.275 Å⁻¹ spacing in parallel momentum space established as the low-density striped phase conformation.⁹ We believe this to be an ($8.3\times\sqrt{3}$) structure based on the reconstructed ($23\times\sqrt{3}$) Au nearest neighbor spacing as discussed in our prior work.²⁸ The representative inelastic spectrum in Fig. 3(b) shows two dispersionless modes at $\Delta E = 7.3\pm 0.4$ and 12.3 ± 0.4 meV. The lower energy mode we assign to the FT_z mode found in the longer chain alkanethiol systems. We attribute the higher energy mode, which is also dispersionless [see Fig. 3(c)], to the first overtone of the 7.3 meV FT_z phonon. This overtone assignment is discussed later.

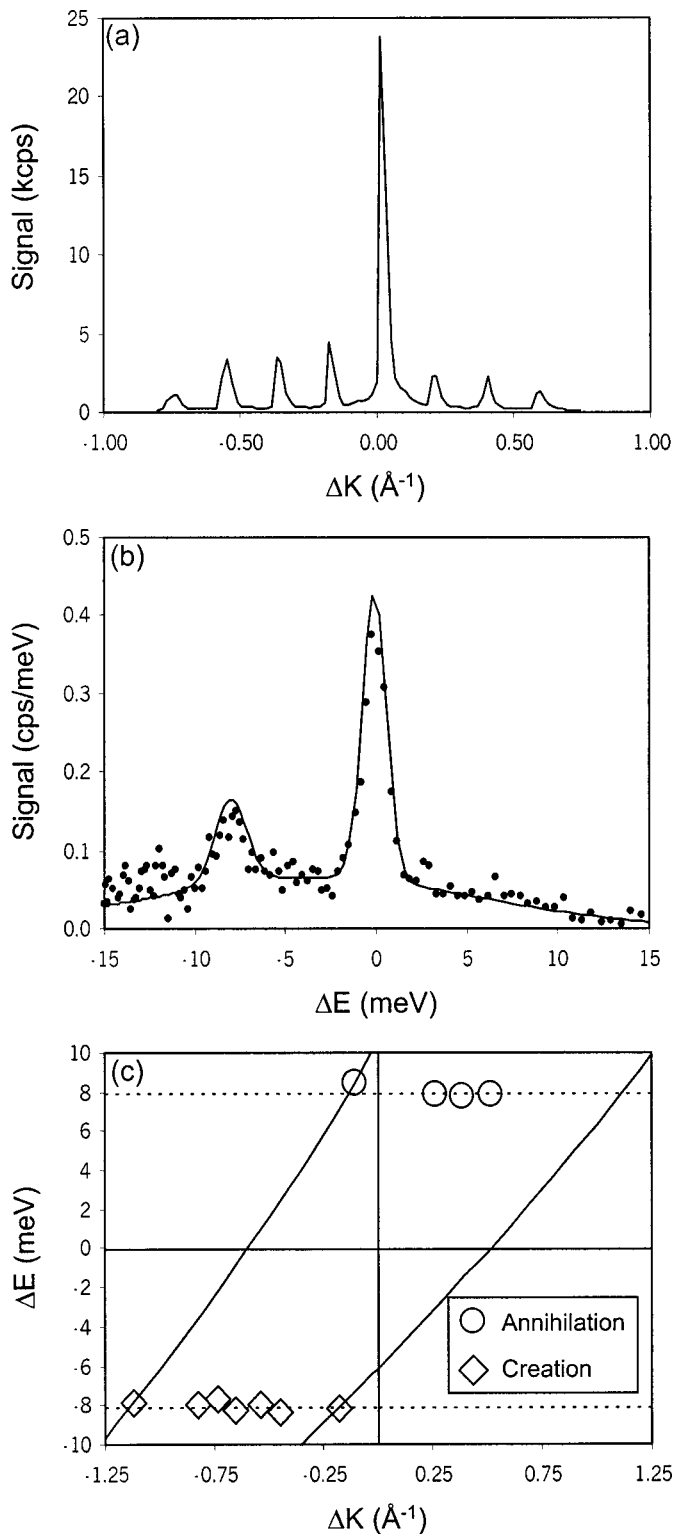


FIG. 1. (a) Helium diffraction scan of the $(11.5 \times \sqrt{3})$ C10 phase in the $\langle 110 \rangle$ direction. (b) Representative time of flight data from the C10 striped phase taken with a 32.31 meV beam, 100 K surface temperature, and incident and final angles of 36.02° and 36.82° , respectively. The solid line is a least squares fit of the data points. (c) A C10 ΔK vs ΔE dispersion plot showing the creation and annihilation events. The solid lines are selected scan curves taken at $\theta_i = 36.02$ with $\theta_f = 30.82$ and 40.82 ; the dashed lines are the average value of the phonon energy.

The Debye–Waller factor, $W(T_s)$, was extracted from the C6 data by measuring the integrated specular peak intensity as function of the surface temperature, which was incre-

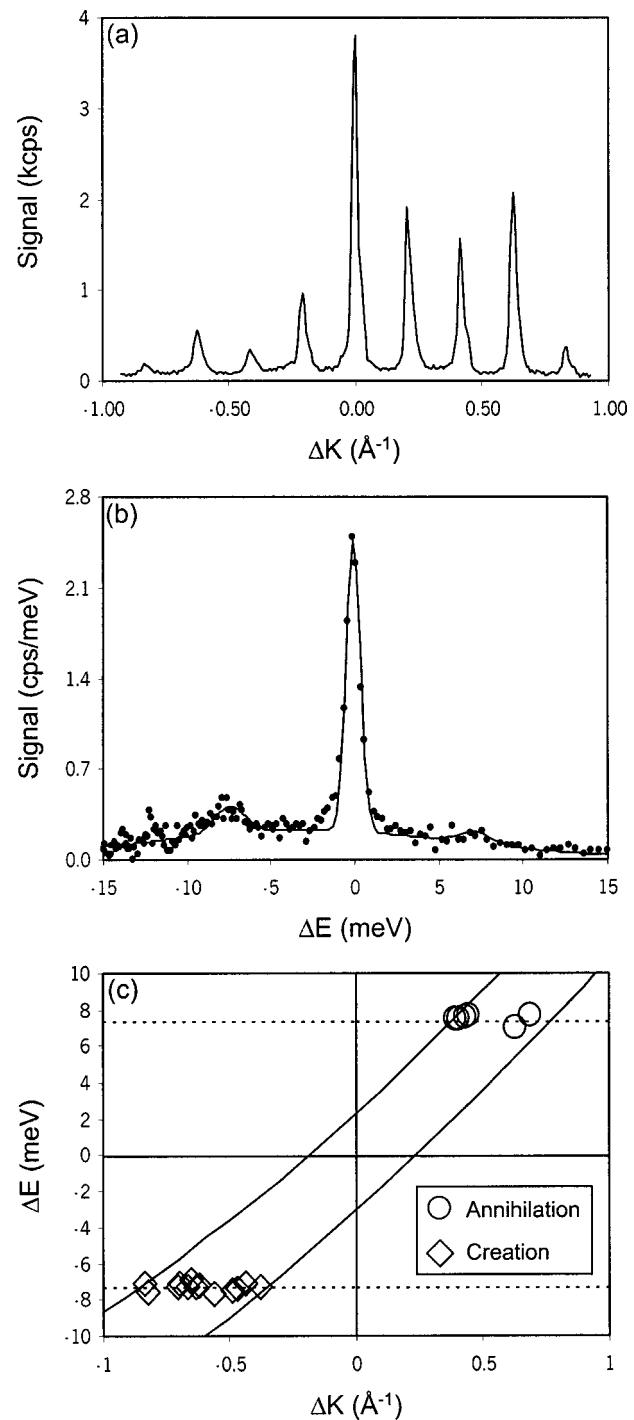


FIG. 2. (a) Helium diffraction scan of the $(10 \times \sqrt{3})$ C8 phase in the $\langle 110 \rangle$ direction. (b) Representative time of flight data from the C8 striped phase taken with a 26.92 meV beam, 100 K surface temperature, and at a range of incident and final angles. The solid line is a least squares fit of the data points. (c) A C8 ΔK vs ΔE dispersion plot showing the creation and annihilation events. The solid lines are selected scan curves taken at $\theta_i = 36.92$ and 35.92 with $\theta_f = 38.92$ and 33.92 , respectively; the dashed lines are the average value of the phonon energy.

mentally increased, at three different incident beam angles. The peak intensity is related to $W(T_s)$ by

$$I = I_0 e^{-2W(T_s)}, \quad (2)$$

where I is the reflected peak intensity and I_0 is the peak intensity at a surface temperature of 0 K. The Debye–Waller

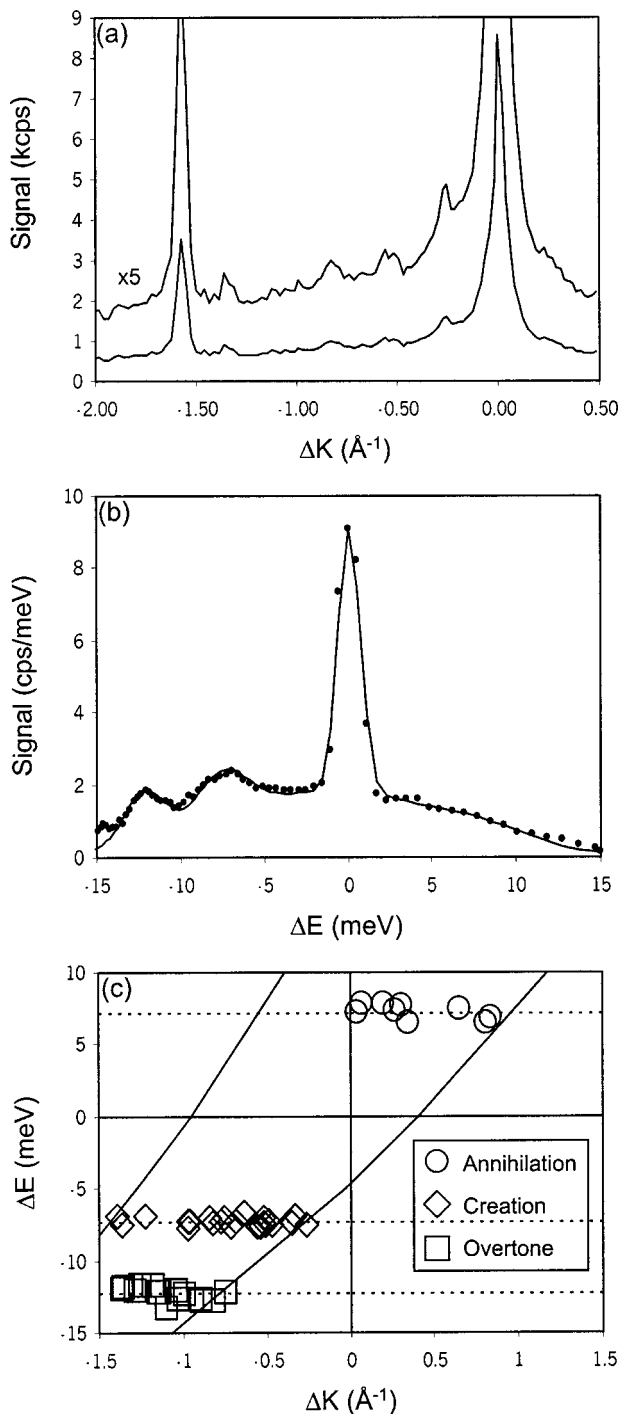


FIG. 3. (a) Helium diffraction scan of the $(8.3 \times \sqrt{3})$ C6 phase in the $\langle 110 \rangle$ direction. (b) Representative time of flight data from the C6 striped phase taken with a 28.00 meV beam, 100 K surface temperature, and at a range of incident and final angles. The solid line is a least squares fit of the data points. (c) A C6 ΔK vs ΔE dispersion plot showing the creation and annihilation events for the fundamental and creation event for the overtone FT_z phonon. The solid lines are selected scan curves taken at $\theta_i = 35.92$ with $\theta_f = 29.92$ and 39.92 ; the dashed lines are the average value of the phonon energy.

factor has components from the normal and parallel momentum transfers, Δk_z and Δk_{\parallel} , and mean square displacements, $\langle U_z^2 \rangle$ and $\langle U_{\parallel}^2 \rangle$,

$$2W(T_s) = \Delta k_z^2 \langle U_z^2 \rangle + \Delta k_{\parallel}^2 \langle U_{\parallel}^2 \rangle. \quad (3)$$

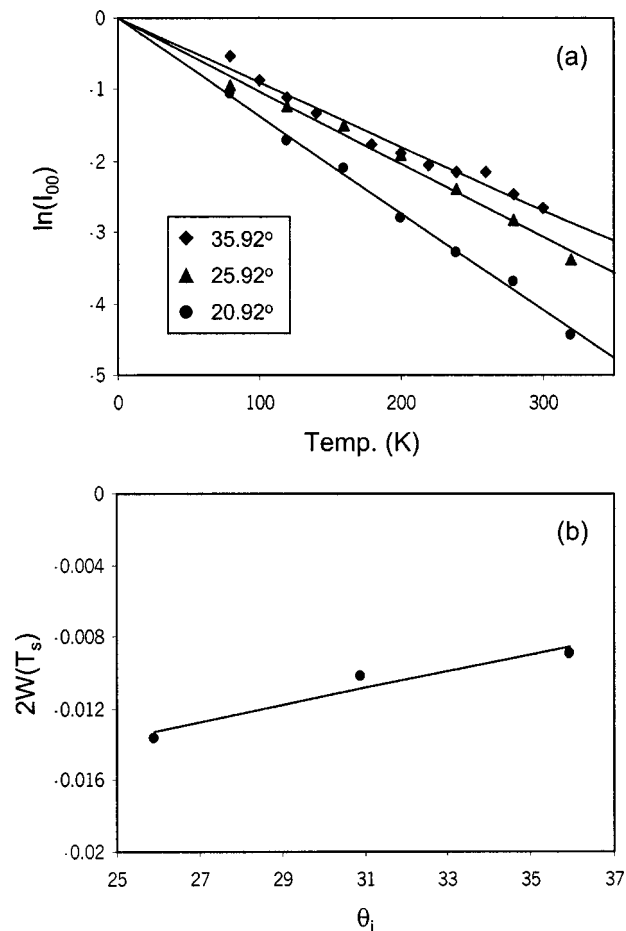


FIG. 4. (a) Plot used to determine the Debye–Waller factor, $W(T_s)$. The lines through the data are linear regressions giving a slope for different incident scattering angles. (b) The three $W(T_s)$ values as a function of incident angle, θ_i . The line is a linear regression fit used to determine the $d\langle U_z^2 \rangle/dT$.

The specular diffraction peak has no contribution from Δk_{\parallel} , forcing one of the above terms to zero. The expression for Δk_z is given by

$$\Delta k_z = k_i \left[\left(\cos^2 \theta_i + \frac{D}{E} \right)^{1/2} + \left(\cos^2 \theta_f + \frac{D}{E} \right)^{1/2} \right]. \quad (4)$$

The Beeby²⁹ correction, D , accounts for the added attractive potential between the He atom and the surface. E and θ are the kinetic energy of the He atom and incident or final angle from surface normal. Using the Debye–Waller factor and a Beeby correction of 8 meV taken from prior theoretical work on SAMs,¹⁵ the mean square displacement perpendicular to the surface can be determined as a function of temperature, $d\langle U_z^2 \rangle/dT$. Figure 4(a) shows the normalized natural log of the signal (background contribution subtracted) versus surface temperature plots from which the Debye–Waller factors were extracted. Figure 4(b) shows $W(T_s)$ as a function of incident angle, used to better characterize the Δk_z in extracting the mean square displacement. The perpendicular mean square displacement calculated for C6/Au(111) is $0.68 \times 10^{-4} \text{ \AA}^2 \text{ K}^{-1}$, as compared to our value of $2.16 \times 10^{-4} \text{ \AA}^2 \text{ K}^{-1}$ for C10/Au(111). A similar value of $1.40 \times 10^{-4} \text{ \AA}^2 \text{ K}^{-1}$ was reported for C11/Au(111).³⁰

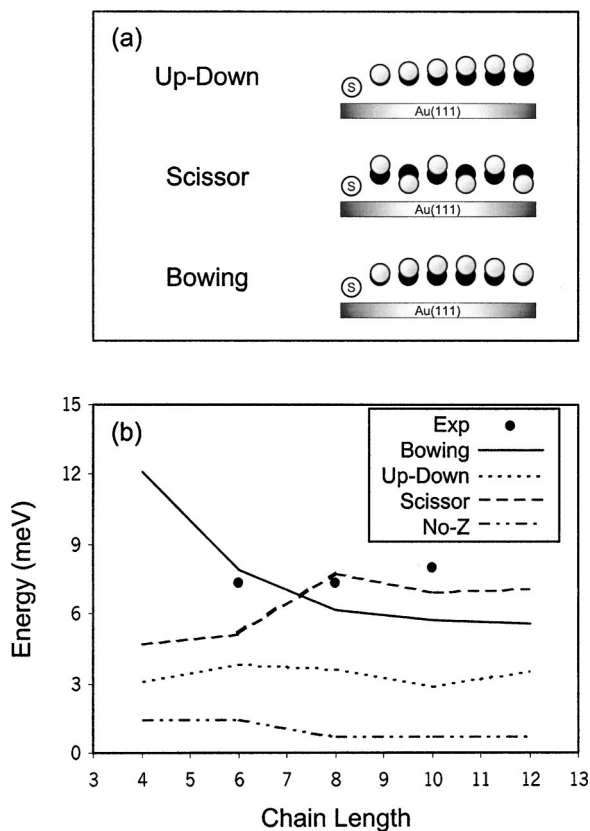


FIG. 5. (a) Sketch showing VENUS generated low-energy normal mode z displacements from the equilibrium position for C6. The solid circles represent the equilibrium position; the open circles represent the maximum displacement; the circle with an S is the sulfur. (b) VENUS generated low-energy modes and experimentally found phonon energies for differing chain length as a function of carbon units. Four different theoretical modes are shown, a scissor, a bowing motion, an up-down mode, and a non- z -polarized mode.

VENUS calculations revealed three distinct low energy modes, with polarization components normal to the surface, which were common for all chain lengths; an up-down motion, a scissor, and a bowing motion. Figure 5(a) graphically depicts the equilibrium position and an extremum of each mode for a C6 molecule, which is representative for all modeled chain lengths. The calculated energies of the three low-energy modes as a function of the chain length are compared to the experimental energies in Fig. 5(b). In addition, a low-energy mode parallel to the surface, which is a wag in the plane parallel to the surface, is also included in Fig. 5(b). The normal modes analysis was focused on modes with large z -polarizations because of the experimentally observed FT_z mode. The planar theoretical modes do, however, demonstrate trends in the vibrational frequency due to chain length.

IV. DISCUSSION

The FT_z modes for C6, C8, and C10 on Au(111) can be modeled by van der Waals forces between the surface and the hydrocarbon chain. The relationship between the FT_z vibrational frequency and chain length in this class of systems agrees in part with prior work on alkanes and physisorbed alkanethiols.^{19,20} Witte *et al.* showed that alkanes of varying chain length on Cu(111) had essentially the same vibrational

energies and further explored the Einstein mode by deuterating n -octane. The scaling of the vibrational energy of n -octane to deuterated n -octane showed an excellent agreement with a simple force constant approximation, $E \approx \sqrt{k/m}$. The work was then expanded to alkanethiols, 1-heptanethiol and ethanethiol, physisorbed on Cu(111) where a 6 meV FT_z mode was found, again showing no dependence on chain length.

In our study of chemisorbed alkanethiols, the C6 and C8 modes appear, not surprisingly, to be equivalent. For each additional methyl group added to the chain the force constant, k , and mass, m , will increase in proportion keeping the excitation energy, E , constant, with a small perturbation due to the effective mass of the sulfur head group. The equivalence of the C6 and C8 modes implies that the FT_z mode is similar to those in the alkanes on Cu(111) and can be modeled by the simplest of attractions between that of the methyl groups and Au(111).

The difference in vibrational frequency between the physisorbed alkanethiols on Cu and chemisorbed SAMs on Au(111) is likely due to a combination of effects. The chemical bond of the sulfur group to the surface more tightly binds the nearest methyl groups, thereby increasing the overall vibrational energy. The substrates also play a role in the shift due to their different van der Waals radii. Experiments on chemisorbed alkanethiols on vicinal Cu surfaces show no external vibrational modes, though this may be due to a variety of factors, including a larger sulfur substrate binding energy and a $\sim 13^\circ$ tilt angle.²⁰

In contrast to the other molecules, C10 does not conform to the expected trend ($E_{C10} = 8.0$ meV, $E_{C8} = 7.3$ meV, $E_{C6} = 7.3$ meV). The C10 mode has a slightly higher energy, enough to provoke further investigation with the VENUS normal modes program. The theoretical study was used to look for any qualitative trend in vibrational energy with respect to chain length. A quantitative agreement was not expected due to the simplicity of the model. Using a single chain removed any constraint to the movement parallel to the surface normally introduced by neighboring or overlapping alkanethiols. The relaxed state of the simulated thiol most likely yielded a lower overall vibrational energy, yet trends in the energy of the sagittally-polarized vibrational modes due to chain length should remain the same. The low-energy modes polarized normal to the surface extracted from VENUS are shown schematically in Fig. 5(a) and include an up-down motion, a scissor, and a bowing motion. These modes, shown in Fig. 5(b) along with a non- z -polarized mode, have no discernable trend with respect to chain length.

The increased experimental energy of the C10/Au mode indicates that this striped phase is more tightly bound to the surface. One possible explanation for the increased binding energy is a long-range commensurate structure that adds to the van der Waals forces between the hydrocarbon chains and the Au(111). We have previously demonstrated that 1-decanethiol has a unique unit cell that matches the underlying reconstructed Au(111).²⁸ The $(23 \times \sqrt{3})$ unit cell of the reconstructed Au(111) coincides with that of twice the C10 repeat spacing, but no commensurate relation exists for the

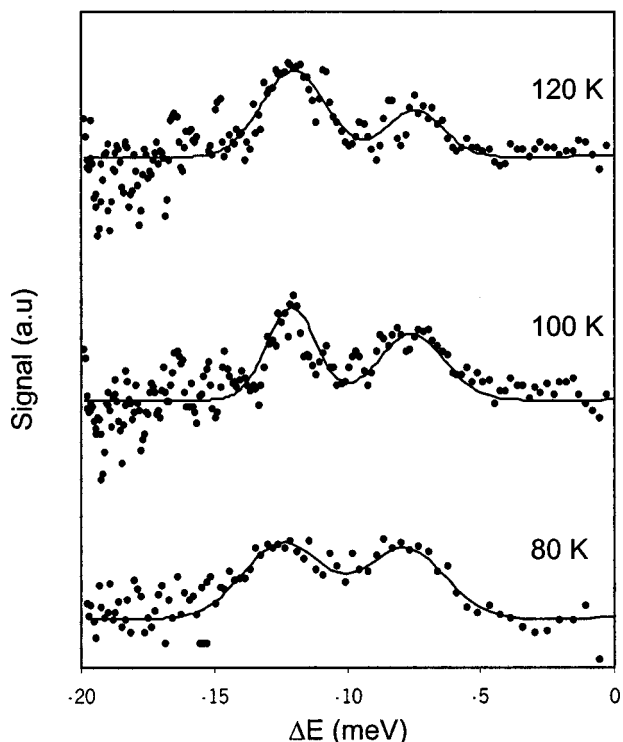


FIG. 6. A comparison of the C6 FT_z mode and overtone with respect to temperature. The data were collected with a 28.5 meV beam at a variety of angles. The solid circles are the data after the multiphonon background and diffuse elastic peaks have been subtracted out, the lines are Gaussian fits to the phonons.

C6 or C8 unit cells. [The theoretical calculations assumed a deconstructed Au(111) surface and, hence, would not account for the extra binding.] The relatively small shift in the energy of the C10 vibration suggests that the increase in the van der Waals intermolecular forces is due to a commensurate structure.

The higher energy C6 phonon, exhibited in Figs. 3(b) and 3(c), was assigned by comparing its intensity to that of the fundamental excitation as a function of temperature. A simple relationship between the probability of the m th phonon transition for oscillators and the surface temperature has been developed,³¹

$$P_m = \exp(-2W(T_s)) \frac{(2W(T_s))^m}{m!}. \quad (5)$$

The parameter m is the order of excitation and $W(T_s)$ is the Debye–Waller factor determined for C6/Au(111). This relationship has been used effectively for prior work on noble gases on Ag(111).³² The Debye–Waller factor we derived for specular scattering does not account for the parallel mean square displacement and a fitting parameter was used to account for the parallel displacement in the probability calculations. Figure 6 depicts the experimental dependence of the intensity of the C6/Au phonon modes with respect to surface temperature. The background (linear, multiphonon, and diffuse elastic) has been subtracted to allow for easier comparison. Both the experimental and theoretical ratios of the overtone to the first excitation grow linearly with a slope of W as the surface temperature increases. The agreement between

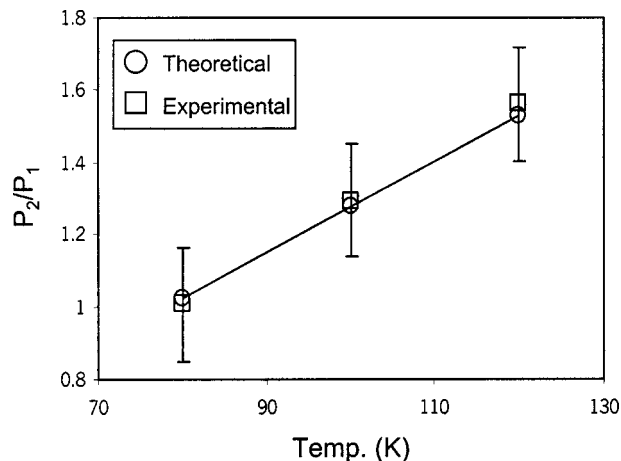


FIG. 7. A plot of the experimental ratios of the probabilities of the overtone to the FT_z mode and a theoretical calculation of the ratios. The data are from a 28.5 meV beam with surface temperatures of 80, 100, and 120 K. The theoretical data use the experimentally determined $d\langle U_z^2 \rangle/dT$ plus a fitting parameter to account for the parallel mean square displacement.

the experiment and predicted probability, shown in Fig. 7, along with prior observations of FT_z overtones in alkanes and similar physisorbed systems lead to the assignment of the higher energy C6 phonon as an overtone.¹⁹ The discrepancy between the expected energy, i.e., twice that of the first excitation, and the observed energy likely is due to anharmonicity. The lack of an overtone for C8 and C10 is likely due to their larger Debye–Waller factors, which would decrease the overall probability, P_m .

V. CONCLUSION

We have performed a series of experimental and simulation studies in order to dissect the forces driving the self-assembly of alkanethiolate monolayers. The striped phases of 1-decanethiol, 1-octanethiol, and 1-hexanethiol exhibit FT_z phonons at 8.0, 7.3, and 7.3 meV, respectively. The 12.3 meV overtone for the C6/Au(111) striped phase is assigned as the excitation of the FT_z mode. Alkanethiols on Au(111) exhibit a distinct single phonon inelastic scattering event with a largely invariant energy. The qualitative molecular dynamics simulations also suggest that the frequencies of the low energy vibrations are relatively constant with respect to chain length. The interactions responsible for these phonons are driven by the van der Waals forces between the methylene/methyl groups and the Au substrate atoms. We also suggest that the modestly increased energy of the C10 mode with respect to C8 and C6 comes from increased binding due to the commensurate structure that C10 has with respect to the Au(111) reconstruction. This work represents a step forward in understanding the forces that govern interfacial self-assembly.

ACKNOWLEDGMENTS

We thank Kevin Gibson and Bill Isa for their insightful thoughts and discussions on the VENUS code and inelastic scattering of helium from alkanethiol monolayers. We would also like to thank Ken Nicholson and Yi Wang for their ideas,

time, and support. This work was primarily supported by the Chemical Sciences, Geosciences and Biosciences Division, Office of Basic Energy Sciences, Office of Science, U.S. Department of Energy, Grant No. DE-FG02-00ER15089. We also acknowledge the Burroughs Wellcome Fund Interfaces Cross-Disciplinary Training Program at the University of Chicago for partial support of the computer cluster, as well as supplemental infrastructure support from the NSF-Materials Research Science and Engineering Center at the University of Chicago, NSF-DMR-0213745. M.A.F. gratefully acknowledges support through a National Science Foundation Graduate Research Fellowship.

- ¹A. Ulman, *Chem. Rev.* **96**, 1533 (1996).
- ²F. Schreiber, A. Eberhardt, T. Y. B. Leung, P. Schwartz, S. M. Wetterer, D. J. Lavrich, L. Berman, P. Fenter, P. Eisenberger, and G. Scoles, *Phys. Rev. B* **57**, 12476 (1998).
- ³G. E. Poirier, *Langmuir* **15**, 1167 (1999).
- ⁴N. Camillone, T. Y. B. Leung, and G. Scoles, *Surf. Sci.* **373**, 333 (1996).
- ⁵S. B. Darling, A. W. Rosenbaum, and S. J. Sibener, *Surf. Sci.* **478**, L313 (2001).
- ⁶*An Introduction to Ultrathin Organic Films: From Langmuir-Blodgett to Self-Assembly*, edited by A. Ulman (Academic, Boston, 1991).
- ⁷G. M. Whitesides and P. E. Laibinis, *Langmuir* **6**, 87 (1990).
- ⁸L. H. Dubois and R. G. Nuzzo, *Annu. Rev. Phys. Chem.* **43**, 437 (1992).
- ⁹N. Camillone, T. Y. B. Leung, P. Schwartz, P. Eisenberger, and G. Scoles, *Langmuir* **12**, 2737 (1996).
- ¹⁰D. Fuhrmann and C. Wöll, *New J. Phys.* **1**, 1.1 (1998).
- ¹¹D. Fuhrmann and C. Wöll, *Surf. Sci.* **377-379**, 544 (1997).
- ¹²F. Y. Hansen and H. Taub, *Phys. Rev. Lett.* **69**, 652 (1992).
- ¹³D. Fuhrmann, R. Gerlach, H. G. Rubahn, and C. Wöll, *Surf. Sci.* **424**, 145 (1999).
- ¹⁴S. B. M. Bosio and W. L. Hase, *J. Chem. Phys.* **107**, 9677 (1997).
- ¹⁵N. Camillone, C. E. D. Chidsey, G.-y. Liu, T. M. Putvinski, and G. Scoles, *J. Chem. Phys.* **94**, 8493 (1991).
- ¹⁶S. M. Wetterer, D. J. Lavrich, T. Cummings, S. L. Bernasek, and G. Scoles, *J. Phys. Chem. B* **102**, 9266 (1998).
- ¹⁷W. L. Manner, A. R. Bishop, G. S. Girolami, and R. G. Nuzzo, *J. Phys. Chem. B* **102**, 8816 (1998).
- ¹⁸G. Witte and C. Wöll, *J. Chem. Phys.* **103**, 5860 (1995).
- ¹⁹G. Witte, D. Fuhrmann, and C. Wöll, *Chem. Phys. Lett.* **265**, 347 (1997).
- ²⁰S. Vollmer, P. Fouquet, G. Witte, C. Boas, M. Kunat, U. Burghaus, and C. Wöll, *Surf. Sci.* **462**, 135 (2000).
- ²¹B. Gans, S. F. King, P. A. Knipp, D. D. Koleske, and S. J. Sibener, *Surf. Sci.* **264**, 81 (1992).
- ²²L. Niu, D. D. Koleske, D. J. Gaspar, and S. J. Sibener, *J. Chem. Phys.* **102**, 9077 (1995).
- ²³W. L. Hase, R. J. Duchovic, X. Hu *et al.*, *QCPE* **16**, 671 (1996).
- ²⁴T. Yan and W. L. Hase, *J. Phys. Chem. A* **105**, 2617 (2001).
- ²⁵T. K. Xia, J. Ouyang, M. W. Ribarsky, and U. Landman, *Phys. Rev. Lett.* **69**, 1967 (1992).
- ²⁶Y. Yourdshahyan, H. K. Zhang, and A. M. Rappe, *Phys. Rev. B* **63**, 081405(R) (2001).
- ²⁷F. Schreiber, *Prog. Surf. Sci.* **65**, 151 (2000).
- ²⁸S. B. Darling, A. W. Rosenbaum, Y. Wang, and S. J. Sibener, *Langmuir* **18**, 7462 (2002).
- ²⁹J. L. Beeby, *J. Phys. C* **4**, L359 (1971).
- ³⁰P. V. Schwartz, D. J. Lavrich, and G. Scoles, *Langmuir* **19**, 4969 (2003).
- ³¹H.-D. Meyer, *Surf. Sci.* **104**, 117 (1981).
- ³²K. D. Gibson and S. J. Sibener, *J. Chem. Phys.* **88**, 7862 (1988).